

Chiral Magnetic Effect in Protoneutron Stars and Magnetic Field Spectral Evolution

Günter Sigl and Natacha Leite

II. Institut für Theoretische Physik, University of Hamburg
Luruper Chaussee, 149, 22761 Hamburg, Germany

E-mail: guenter.sigl@desy.de, natacha.leite@desy.de

Abstract. We investigate the evolution of the chiral magnetic instability in a protoneutron star and compute the resulting magnetic power and helicity spectra. The instability may act during the early cooling phase of the hot protoneutron star after supernova core collapse, where it can contribute to the buildup of magnetic fields of strength up to the order of 10^{14} G. The maximal field strengths generated by this instability, however, depend considerably on the temperature of the protoneutron star, on density fluctuations and turbulence spectrum of the medium. At the end of the hot cooling phase the magnetic field tends to be concentrated around the submillimeter to cm scale, where it is subject to slow resistive damping.

Contents

1	Introduction	1
2	Framework and basic equations	2
2.1	Thermodynamics of a protoneutron star	2
2.2	Evolution equations	3
2.3	Magnetic field amplification	5
2.4	Energy balance	6
2.5	Density fluctuations	8
3	Solutions of the evolution equations	9
3.1	Neutrino sphere and cold neutron star	12
4	Summary and conclusions	14
A	The role of turbulence	15

1 Introduction

The origin of the magnetic field strengths observed in neutron stars and magnetars (highly magnetized neutron stars [1]) up to 10^{15} G [2, 3] is still under debate. The most popular explanations include adiabatically compressed fossil fields of the parent star and dynamo generated fields [4]. More recently it has been suggested that the magnetic field of magnetars is related to a chiral asymmetry of particles, produced during the core collapse of supernovae [5]. An imbalance in the number of right- and left-handed fermions was previously studied in the context of QCD plasmas [6, 7] as well as applied to the early universe as a possibility to explain the generation and evolution of cosmological magnetic fields [8, 9]. This so-called chiral magnetic effect or chiral magnetic instability was also suggested to account for the observed kicks that accelerate neutron stars [10].

In a pure electron-positron plasma, the chiral magnetic instability does not allow the growth of seed magnetic fields [11], but in the presence of neutrinos an electroweak plasma with neutrino-antineutrino asymmetries was found to be able to amplify magnetic fields to interesting scales for neutron stars [12, 13]. Another crucial ingredient to take into account are the spin flip interactions due to the finite electron mass which violates chirality. This tends to decrease the asymmetry between left- and right-handed electrons faster than it is created by electroweak processes [14]. In addition, it was claimed that the chiral asymmetry in the forward scattering amplitude of electrons off nuclei due to the electroweak interaction can create a magnetic field instability in the same way that the chiral asymmetry does, but which acts on much longer time scales and is not washed out by chirality-flipping processes [15, 16].

It is not yet clear if the chiral magnetic instability can transfer sufficient energy stored in chiral fermions into magnetic field energy to give a significant contribution to the magnetic fields inferred for neutron stars and magnetars. In the present paper we aim to model the chiral magnetic effect in this environment, review the underlying assumptions proposed for this mechanism to work and understand its physical implications. We solve the evolution

equations for the chiral chemical potential, the chemical potential of the background species on which electrons scatter, the magnetic energy and the magnetic helicity power spectra. This allows us to estimate the conditions for which magnetic fields can be amplified in a neutron star. We show that a seed magnetic field can be amplified to small scales shortly after the collapse in the core of hot stars through the chiral magnetic effect and that for its surface or cooled down neutron stars this mechanism is not effective to generate the strong magnetic fields observed.

The remainder of the paper is structured as follows: In Sect. 2 we summarize the conditions in a protoneutron star relevant for magnetic field evolution and set up the basic modified MHD equations. In Sect. 3 we solve the evolution equations, estimate the maximal magnetic field strength and discuss assumptions and uncertainties. We summarize our results and conclude in Sect. 4. Throughout the paper we will use Gaussian natural units, $c_0 = \hbar = k_B = 1$, and the electric permittivity and magnetic permeability of the vacuum are set to $\epsilon_0 = 1/(4\pi)$ and $\mu_0 = 4\pi$, respectively.

2 Framework and basic equations

2.1 Thermodynamics of a protoneutron star

Immediately after core collapse, a protoneutron star reaches temperatures of the order of tens of MeV in its core. To a given temperature corresponds a chemical potential $\Delta\mu = \mu_n - \mu_p = \mu_e - \mu_\nu$ [17], that can be used together with the fact that neutrinos are trapped inside the core at this stage, such that the lepton fraction Y_L is temporarily conserved. The relation $Y_L n_B = n_e + n_\nu$, where $n_B = n_n + n_p$ is the baryon number density, and electric neutrality, $n_e = n_p$, allows us to estimate the number densities and chemical potentials of the particle species involved.

When a massive star collapses protons are converted into neutrons by capturing left-handed electrons $e_L + p \rightarrow n + \nu_{eL}$, producing an asymmetry between the number of left- and right-handed electrons $N_5 \equiv N_L - N_R$. Such electroweak reactions are known as URCA processes and their emissivity is [18]

$$\epsilon_{\text{URCA}} = \frac{457\pi}{10080} (1 + 3g_A^2) \cos^2 \theta_C G_F^2 m_n m_p \mu_e T^6, \quad (2.1)$$

where $g_A \simeq 1.26$ is the axial-vector coupling of the nucleon, $\theta_C \approx 0.24$ is the Cabbibo angle, $G_F = 1.166 \times 10^{-5} \text{ GeV}^{-2}$, m_n and m_p are the masses of the neutron and proton, respectively and μ_e is the electron chemical potential. Since $\mu_e \gg T$, the rate of electron capture is then

$$\Gamma_w = \frac{\epsilon_{\text{URCA}}}{\mu_e Y_L n_B}. \quad (2.2)$$

If the URCA processes are not in thermodynamic equilibrium with the inverse reactions, an asymmetry N_5 can build up. This is the case, for example, if neutrinos escape the neutron star, which occurs when their mean free path is larger than the neutron star radius. This condition is met beyond the neutrino sphere or when enough time has passed for the star to cool down to the point when it becomes transparent to neutrinos, roughly 10 seconds after collapse.

For the typical momenta of the particles in the core of a protoneutron star electron capture takes place, while in the crust or when proton and electron concentrations are low

momentum conservation highly suppresses electron capture and an additional particle is required to absorb momentum, such as another proton or neutron. If $p_{F,n} > p_{F,e} + p_{F,p}$, the previous rate is modified to [19]

$$\Gamma_w^{\text{mod}} \simeq \frac{11513\pi}{120960} \alpha_\pi^2 G_F^2 \cos \theta_C g_A^2 \frac{T^8}{Y_L n_B}, \quad (2.3)$$

where $\alpha_\pi \approx 15$ is the pion-nucleon fine structure constant.

During the hot initial phase, the charge carriers in the neutron star are semi-degenerate. There are no simple equations for the conductivity for this case. In the degenerate limit the conductivity is given by the following expression [20],

$$\sigma \simeq 1.5 \times 10^{45} \left(\frac{\text{K}}{T} \right)^2 \left(\frac{\rho_p}{10^{13} \text{ g cm}^{-3}} \right)^{3/2} \text{ s}^{-1}, \quad (2.4)$$

with ρ_p the proton density. In the relativistic non-degenerate high temperature limit the conductivity would be dominated by the pair plasma and be of the order of the temperature [21] which is lower than the obtained through (2.4). However, it turns out that the final magnetic field is insensitive to the conductivity in this range of values because the magnetic field grows on timescales much shorter than the dynamical timescale of the system and then saturates. Therefore, for our calculations we will use eq. (2.4) for the conductivity, which is closer to the relevant conditions in the protoneutron star, and we will also assume the temperature T and the conductivity σ to be constant.

Even though in the core of a collapsing supernova electrons are relativistic, the fact that they are massive suggests that we should not take them as strictly chiral particles, since the amplitude of a positive helicity component for a left-chiral state is approximately $(E + m_e - p)/(E + m_e) \simeq (m_e/E)$. This means that there is a probability $(m_e/E)^2$ that a scattering electron of a certain chirality flips into the opposite chirality state – either by Rutherford scattering, electron-electron scattering or Compton scattering – which tends to decrease N_5 . Rutherford scattering dominates in this case, which allows us to write the chirality-flipping rate as $(E \sim T)$ [14]

$$\Gamma_f \simeq \frac{e^4 m_e^2}{48\pi^3 \mu_e} \left[\ln \frac{12\pi^2 T}{e^2(3T + \mu_e)} - 1 \right], \quad (2.5)$$

where e is the electron charge and m_e is the electron mass.

2.2 Evolution equations

When a chiral imbalance is present, such as the one originated by electron capture, the Adler-Bell-Jackiw anomaly implies that a current

$$j_5^\mu \equiv \bar{\psi} \gamma^\mu \gamma_5 \psi = j_L^\mu - j_R^\mu \quad (2.6)$$

will be induced, whose partial derivative, instead of vanishing, is related to the Chern-Simons current through

$$\partial_\mu j_5^\mu = \frac{g^2}{32\pi^2} F_{\mu\nu}^\alpha \tilde{F}^{\alpha,\mu\nu} = \partial_\mu K^\mu. \quad (2.7)$$

With $N_5 = \int d^3\mathbf{r} \bar{\psi} \gamma_5 \psi$ and $N_{CS} \equiv \int d^3\mathbf{r} K^0$ space integration implies the conservation relation

$$\frac{d}{dt} (N_5 - N_{CS}) = 0. \quad (2.8)$$

Thus the Chern-Simons number of the electromagnetic field connects the chiral asymmetry to the magnetic helicity

$$\frac{d}{dt} \left(N_5 - \frac{e^2}{4\pi^2} \mathcal{H} \right) = 0, \quad \mathcal{H} = \int d^3\mathbf{r} \mathbf{B} \cdot \mathbf{A}, \quad (2.9)$$

with the magnetic field \mathbf{B} and vector potential \mathbf{A} .

Maxwell's equations are then modified by the introduction of a current contribution

$$\mathbf{j}_5 = -\frac{e^2}{2\pi^2} \mu_5 \mathbf{B} \quad (2.10)$$

in the presence of a chiral imbalance, with chiral chemical potential $\mu_5 \equiv (\mu_L - \mu_R)/2$. This affects the magnetohydrodynamics (MHD) equation that now takes the form

$$\partial_t \mathbf{B} = \nabla \times (\mathbf{v} \times \mathbf{B}) + \eta \Delta \mathbf{B} - \frac{2e^2}{\pi} \eta \mu_5 \nabla \times \mathbf{B}, \quad (2.11)$$

with $\eta = 1/(4\pi\sigma)$ being the resistivity. In the following we will neglect the velocity field \mathbf{v} so that our subsequent analysis applies in the plasma rest frame, provided that the velocity field is sufficiently smooth, which we elaborate in appendix A. It will be left to future work to investigate under which conditions this is a good approximation in the presence of turbulence and other contributions to the velocity such as rotation.

In Fourier space and introducing the expansion of the magnetic field into a left- and right-handed part

$$\tilde{\mathbf{B}}(\mathbf{k}) = b_{\mathbf{k}}^+ \mathbf{h}_{\mathbf{k}}^+ + b_{\mathbf{k}}^- \mathbf{h}_{\mathbf{k}}^-, \quad \mathbf{h}_{\mathbf{k}}^\pm \equiv \frac{1}{\sqrt{2}} \left(\mathbf{e} \pm i \frac{\mathbf{k}}{k} \times \mathbf{e} \right), \quad (2.12)$$

where \mathbf{e} is an arbitrary unit vector perpendicular to \mathbf{k} , one can then rewrite (2.11) as

$$\partial_t b_{\mathbf{k}}^\pm = -\eta k \left(k \pm \frac{2e^2}{\pi} \mu_5 \right) b_{\mathbf{k}}^\pm. \quad (2.13)$$

The magnetic field energy density and helicity density can be written in terms of the power spectra in Fourier space, $M_k \equiv k^3 |\tilde{\mathbf{B}}(\mathbf{k})|^2/2$ and $H_k \equiv -4\pi i k [\mathbf{k} \times \tilde{\mathbf{B}}(\mathbf{k})] \cdot \mathbf{B}^*(\mathbf{k})$, as

$$\begin{aligned} \rho_m &= \frac{1}{V} \int d^3\mathbf{r} \frac{\mathbf{B}^2(\mathbf{r})}{8\pi} = \frac{M_k}{V} \int_0^\infty d \ln k M_k, \\ h &= \frac{1}{V} \int_0^\infty d \ln k H_k. \end{aligned} \quad (2.14)$$

Combining (2.12) and (2.13) and multiplying with the magnetic field complex conjugate, the power spectra evolution is given by

$$\partial_t \rho_m = -\frac{\eta}{V} \int d \ln k k^2 \left(2M_k + \frac{e^2}{2\pi^2} \mu_5 H_k \right), \quad (2.15)$$

$$\partial_t h = -\frac{\eta}{V} \int d \ln k (2k^2 H_k + 32e^2 \mu_5 M_k), \quad (2.16)$$

where V is the volume. We can translate particle number into chemical potential using

$$N_5 = \frac{V}{3\pi^2} \mu_5 (\mu_5^2 + 3\mu_e^2 + \pi^2 T^2), \quad (2.17)$$

which can be approximated to linear order in μ_5 to $N_5 = c(T, \mu_e)V\mu_5$, with

$$c(T, \mu_e) = \frac{\mu_e^2}{\pi^2} + \frac{T^2}{3}. \quad (2.18)$$

To express the evolution of the chiral chemical potential we take into account the processes described by (2.5) and (2.9) that affect the number of left- and right-handed particles, resulting in

$$\partial_t \mu_5 = \frac{e^2}{4\pi^2 c(T, \mu_e)} \partial_t h - 2\Gamma_f (\mu_5 - \mu_{5,b}), \quad (2.19)$$

where $\mu_{5,b}$ is the equilibrium value of μ_5 in the absence of resistivity. This term represents an effective chemical potential generated by the interactions of electrons with background species such as neutrinos that act as sources of the asymmetry, thus containing the term proportional to (2.2). We can roughly estimate it by considering the number N_b of background particles, such that the processes that change N_5 , neglecting the magnetic field contribution for now, can be written as

$$\partial_t N_5 = \pm \Gamma_w N_b - 2\Gamma_f N_5. \quad (2.20)$$

Comparing this with (2.19), results in

$$N_b = 2Vc(T, \mu_e) \frac{\Gamma_f}{\Gamma_w} |\mu_{5,b}|. \quad (2.21)$$

Furthermore, we approximate the background particles at the temperatures of the core of a protoneutron star to be non-degenerate relativistic fermions with g_b degrees of freedom. This is plausible since the chiral asymmetry mostly results from URCA processes involving chiral neutrinos whose chemical potential is at most of the order of the temperature which would give rise to order one corrections. From thermodynamics we can then relate the number of background particles with the temperature using $N_b = 3\zeta(3)Vg_b T^3/(2\pi)^2$, yielding

$$|\mu_{5,b}| = \frac{3\zeta(3)}{8\pi^2} g_b \frac{\Gamma_w}{\Gamma_f} \frac{T^3}{c(T, \mu_e)}. \quad (2.22)$$

This effective background chemical potential can also include a possible contribution from the difference of the forward scattering amplitudes of left- and right-handed electrons on nucleons, that was considered in the form of an effective potential V_5 in [15] and [16]. Requiring energy conservation of the combined system consisting of the magnetic field, the chiral asymmetry in the electro sector and the background particles implies an evolution equation for $\mu_{5,b}$ of the form of

$$\partial_t \mu_{5,b} = \Gamma_w \frac{\mu_5}{\mu_{5,b}} (\mu_5 - \mu_{5,b}), \quad (2.23)$$

as we will see below.

2.3 Magnetic field amplification

The initial magnetic field of a protoneutron star, which for example can result from adiabatic compression of the stellar seed field during collapse, is affected by the chiral magnetic effect in a way which depends on the scales we are interested in. From (2.13) for growing modes we obtain the condition

$$k < \frac{2e^2}{\pi} |\mu_5| \equiv k_5(\mu_5), \quad (2.24)$$

such that magnetic field modes with $k > k_5$ decay due to resistivity. For $k < k_5$ the magnetic field mode with the same sign for helicity and μ_5 also decays while the mode with helicity signs opposite to μ_5 grow. All magnetic field modes are damped due to finite resistivity with the resistive damping rate $\Gamma_r = \eta k^2$ whereas the growth/decay rate due to the chiral instability is given by

$$\Gamma_\chi(k) = \frac{2e^2}{\pi} \eta k |\mu_5| = \frac{k_5}{k} \Gamma_r. \quad (2.25)$$

The maximal total growth rate $\Gamma_{\text{tot}} = \Gamma_\chi - \Gamma_r$ occurs at $\Gamma_{\text{max}} = \eta k_5^2/4$, which corresponds to the wavenumber $k_5/2$.

Let us analytically analyze the expected behavior of μ_5 by setting $\partial_t \mu_5 = 0$ in (2.19). If we normalize H_k to the maximal value that the helicity can take, $H_{\text{max}}(k) = 8\pi M_k/k$, this gives

$$\tilde{\mu}_5 = \frac{\Gamma_f \mu_{5,b} - 2\eta e^2 [\pi V c(T, \mu_e)]^{-1} \int d \ln k k M_k (H_k/H_{\text{max}})}{\Gamma_f + 4\eta e^4 [\pi^2 c(T, \mu_e)]^{-1} \rho_m}. \quad (2.26)$$

When the magnetic field is negligible, $\tilde{\mu}_5 \simeq \mu_{5,b}$, and modes smaller than k_5 grow exponentially at the rate Γ_{tot} . The magnetic field terms begin to dominate when $\rho_m \gtrsim \pi^2 c(T, \mu_e)/(4\eta e^4) \Gamma_f$. In this limit the flipping rate is negligible compared to the magnetic field induced rate and the instability yields

$$\tilde{\mu}_5 \simeq -\frac{\pi}{2e^2 \rho_m} \int d \ln k k \frac{M_k}{V} \frac{H_k}{H_{\text{max}}}. \quad (2.27)$$

In general $\tilde{\mu}_5 \neq \mu_{5,b}$ and the terms of (2.19) compensate each other. As a consequence the magnetic helicity density will change linearly with time at a rate

$$\partial_t h \simeq \frac{8\pi^2 c(T, \mu_e)}{e^2} \Gamma_f (\mu_5 - \mu_{5,b}). \quad (2.28)$$

The fact that we have almost maximal helicity implies that also the magnetic energy density changes linearly with time, either growing or decreasing according to the sign of $(\mu_5 - \mu_{5,b})/h$. The helicity would be constant only if $\Gamma_f = 0$ or if $\mu_5 = \mu_{5,b}$. Assuming that the magnetic energy is concentrated around a characteristic scale $k_0 = k_5(\tilde{\mu}_5)$ and that the helicity is maximal and has opposite sign to $\tilde{\mu}_5$ implies that also ρ_m will be constant. In this case the chiral magnetic instability reaches saturation, where the growth and damping rates compensate each other.

2.4 Energy balance

By definition of a chemical potential the energy E_5 associated with the chiral asymmetry is given by $dE_5 = \mu_5 dN_5$ and with $E_5 = 0$ for $\mu_5 = 0$ results in

$$\rho_5 = \frac{E_5}{V} = \frac{c(T, \mu_e)}{2} \mu_5^2. \quad (2.29)$$

Differentiating this with respect to time, using (2.19) with the helicity normalized to its maximal value and inserting k_5 , we obtain

$$\partial_t \rho_5 = -2\eta \int d \ln k \frac{M_k}{V} \left(k_5 k \text{sgn}(\mu_5) \frac{H_k}{H_{\text{max}}} + k_5^2 \right) - 2c(T, \mu_e) \Gamma_f \mu_5 (\mu_5 - \mu_{5,b}). \quad (2.30)$$

We can also estimate the change in magnetic energy that a finite μ_5 can induce by using that the instability produces maximally helical fields and that, as we have seen, the growth has

its peak at $k_5/2$. Thus $dE_m \simeq k_5 |d\mathcal{H}|/(8\pi)$ and using (2.9) gives $dE_m \simeq V c(T, \mu_e) \mu_5 d\mu_5$. If there is an initial chiral asymmetry μ_{5i} , the increase in magnetic energy density is given by

$$\Delta\rho_m \simeq \frac{c(T, \mu_e)}{2} (\mu_{5i}^2 - \mu_5^2). \quad (2.31)$$

The total energy density

$$\rho_{\text{tot}} = \rho_5 + \Delta\rho_m \simeq \frac{c(T, \mu_e)}{2} \mu_{5i}^2, \quad (2.32)$$

then only depends on the initial value μ_{5i} which implies that the maximal increase in magnetic energy density obeys $\Delta\rho_m \leq \rho_{\text{tot}}$.

Eq. (2.15) can be rearranged into

$$\partial_t \rho_m = -2\eta \int d\ln k k^2 \frac{M_k}{V} \left(1 + \frac{k_5}{k} \text{sgn}(\mu_5) \frac{H_k}{H_{\text{max}}} \right), \quad (2.33)$$

which together with (2.30) provides the rate of change of the total energy

$$\begin{aligned} \partial_t \rho_{\text{tot}} &= \partial_t \rho_m + \partial_t \rho_5 \\ &= -2\eta \int d\ln k \frac{M_k}{V} \left[(k - k_5)^2 + 2k_5 k \left(1 + \text{sgn}(\mu_5) \frac{H_k}{H_{\text{max}}} \right) \right] \\ &\quad - 2c(T, \mu_e) \Gamma_f \mu_5 (\mu_5 - \mu_{5,b}). \end{aligned} \quad (2.34)$$

The term proportional to $\mu_{5,b}$ is responsible for the energy exchange with external particles and we see that apart from it, since the integrand of (2.34) is non-negative, the energy decreases due to chirality flips and finite resistivity. It is strictly conserved only for the case $\tilde{\mu}_5 = \mu_{5,b}$, and if the magnetic energy is concentrated in the mode k_5 and helicity is maximal with opposite sign to $\mu_{5,b}$, which are the same conditions mentioned above for $\partial_t \rho_m = 0$.

Similarly to the energy associated with the chiral particles, the energy density ρ_b associated with the background species is given by $dE_b = \mu_{5,b} dN_b$. Using (2.21), this gives

$$\rho_b = \frac{E_b}{V} = c(T, \mu_e) \frac{\Gamma_f}{\Gamma_w} \mu_{5,b}^2. \quad (2.35)$$

The initial chemical potential of the background species, $\mu_{5,bi}$, gives us a measure of the maximal energy that can be transferred into magnetic energy density

$$\Delta\rho_m \lesssim c(T, \mu_e) \frac{\Gamma_f}{\Gamma_w} \mu_{5,bi}^2. \quad (2.36)$$

For the interactions to conserve energy one has to set $\partial_t \rho_b = -\partial_t \rho_5$ in the absence of magnetic fields and, computing the time derivative of (2.35) and using (2.30), this yields the evolution equation for the background species (2.23). This shows that $\mu_{5,b}$ changes typically with the rate Γ_w and that will be in equilibrium for $\mu_5 = \mu_{5,b}$ when the magnetic field is concentrated around $k_5(\mu_{5,b})$ and has maximal helicity of sign opposite to $\mu_{5,b}$, given by (2.22). Fig. 1 shows the dependence of the ratio Γ_w/Γ_f on the temperature for a protoneutron star.

Once the energy contribution (2.36) is added to (2.34), the only remaining source of energy change is resistive damping. Inserting (2.22) into (2.36), we obtain

$$\rho_m^{\text{max}} = \left(\frac{3\zeta(3)}{8\pi^2} g_b \right)^2 \frac{\Gamma_w}{\Gamma_f} \frac{T^6}{c(T, \mu_e)} \simeq 8.3 \times 10^{-3} \frac{\Gamma_w}{\Gamma_f} \frac{T^6}{c(T, \mu_e)}, \quad (2.37)$$

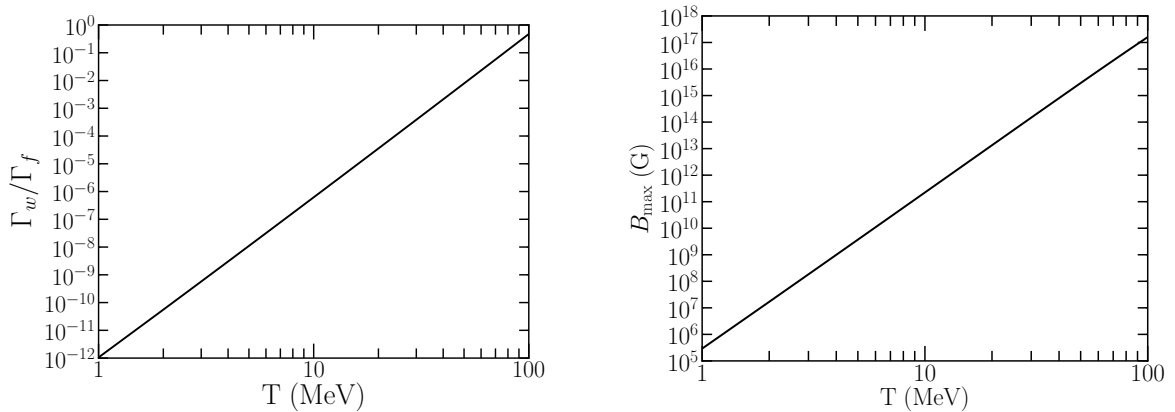


Figure 1. Left panel: The ratio Γ_w/Γ_f obtained using (2.2) and (2.5). Right panel: Estimate maximum magnetic field amplification $B_{\max} = \sqrt{8\pi\rho_m^{\max}}$ due to the chiral magnetic instability as a function of temperature. Logarithmic units to base 10.

where in the last expression the degrees of freedom of the background species were taken as $g_b = 2$. (2.37) can be used to predict the maximal field strength generated for a given temperature and is shown in fig. 1. We can see that the maximal magnetic field amplification strongly increases with temperature.

Up to now we assumed that μ_5 evolves only in time, neglecting the possible contribution of its spatial evolution, as studied by Ref. [22]. There it was shown that the system can be unstable with respect to growing inhomogeneous modes of μ_5 if $k^2/4 > 3e^4 B^2/(8\pi^4 T^2)$ [22]. If we consider the fastest growing mode $k_5/2$ and the maximum magnetic field strength generated from (2.36), we can estimate whether the inhomogeneity of μ_5 plays a role or not in our case. We find then that the solution of (2.19) will be stable if $\Gamma_w/\Gamma_f < 4/\pi$, which is verified for the temperature values we are interested in, as is clear from the left-hand side of Fig. 1. This implies that for our purposes $\mu_5(x, t) \equiv \mu_5(t)$ is a safe and justified assumption.

2.5 Density fluctuations

Neutrinos of energy $E_\nu \simeq 3T$ are trapped at the high temperatures in the protoneutron star core, where densities easily reach $n_B = 2n_0$, with $n_0 \simeq 1.7 \times 10^{38} \text{ cm}^{-3}$ the nuclear matter number density. The mean free path for absorption by a neutron is [23]

$$\ell_{\text{abs}} \simeq 4.5 \times 10^6 \left(\frac{n_0}{n_B}\right)^{2/3} \left(\frac{10 \text{ MeV}}{T}\right)^4 \left[\left(\frac{E_\nu}{T}\right)^4 + 10\pi^2 \left(\frac{E_\nu}{T}\right)^2 + 9\pi^4 \right]^{-1} \text{ cm} \quad (2.38)$$

and the mean free path for scattering with a neutron is

$$\ell_{\text{sca}} \simeq 10^4 \left(\frac{n_0}{n_B}\right)^{1/3} \left(\frac{10 \text{ MeV}}{E_\nu}\right)^2 \frac{10 \text{ MeV}}{T} \text{ cm}. \quad (2.39)$$

The absorption mean free path is more important than scattering and yields $\simeq 1.5 \text{ m}$ for $T = 20 \text{ MeV}$ and $\simeq 10 \text{ cm}$ for $T = 40 \text{ MeV}$. The scattering mean free path yields $\simeq 1 \text{ m}$ at 20 MeV and $\simeq 14 \text{ cm}$ at 40 MeV . These typical temperatures will be used in the following section.

To take into account the fact that the interior of a young neutron star is turbulent we consider the existence of density fluctuations $\delta\rho$ relative to the average density ρ . These density perturbations seem to amount to at least 25% [24]. If the scale of the fluctuations is smaller than the neutrino mean free path, locally these regions can amplify a seed magnetic field, since the neutrinos stream freely on that scale such that the URCA processes and their reverse processes are not in thermal equilibrium and the rate of production of chiral imbalance μ_5 will be of the order of the direct URCA rates Γ_w . To study the influence of the fluctuations somewhat more quantitatively we introduce an effective creation rate of chiral imbalance $\Gamma_w^{\text{eff}} = \Gamma_w \delta\rho/\rho$ which is a rough estimate of the difference of the absorption and emission rates of left chiral electrons due to the electroweak URCA interactions. Rewriting the chiral asymmetry equilibrium value (2.22) and the characteristic wavenumber of the instability (2.24) in terms of the density fluctuations, we have

$$|\mu_{5,b}| = \frac{3\zeta(3)}{8\pi^2} g_b \frac{\delta\rho}{\rho} \frac{\Gamma_w}{\Gamma_f} \frac{T^3}{c(T, \mu_e)}, \quad k_5^{-1} = \frac{4\pi^3 c(T, \mu_e)}{3e^2 \zeta(3) g_b} \left(\frac{\delta\rho}{\rho} \frac{\Gamma_w}{\Gamma_f} T^3 \right)^{-1}. \quad (2.40)$$

From (2.37), the resulting maximal field amplification with respect to the density fluctuations then becomes

$$B_{\text{max}} \simeq \frac{3\zeta(3) g_b}{[8\pi^3 c(T, \mu_e)]^{1/2}} \left(\frac{\delta\rho}{\rho} \frac{\Gamma_w}{\Gamma_f} \right)^{1/2} T^3 \simeq 7.2 \left(\frac{\delta\rho}{\rho} \frac{\Gamma_w}{\Gamma_f} \right)^{1/2} \frac{T^3}{c(T, \mu_e)^{1/2}}. \quad (2.41)$$

3 Solutions of the evolution equations

We now apply the previous treatment to the core and the neutrino sphere of a protoneutron star. In a core collapse supernova with a progenitor mass $\sim 8M_\odot$, as described by [25], shortly after core collapse the lepton fraction is $Y_L \simeq 0.3$. For the chemical potential difference we consider the two realistic cases $\Delta\mu = 80$ MeV and 60 MeV, which correspond to temperatures of $\simeq 40$ MeV and 20 MeV, respectively, for a core density of $2n_0$, as before. We can then compute the number density and chemical potential of each species as described in Sect. 2.1 which results in the electron chemical potential $\mu_e \simeq 260$ MeV and the proton densities $\rho_p \simeq 1.3 \times 10^{14} \text{ g cm}^{-3}$ for 40 MeV and $1.2 \times 10^{14} \text{ g cm}^{-3}$ for 20 MeV. From this the conductivity is obtained from eq. (2.4).

We solve the system of eq. (2.15), (2.16), (2.19) and (2.23) for 90 wavenumber modes spanning from $k_{\text{max}} = 2k_5$ to $k_{\text{min}} = 10^{-4}k_5$, with constant width in $\log_{10} k$. The time scale used is normalized to the resistive damping time of the instability

$$t_{\text{damp}} = \Gamma_\chi^{-1}(k_5) = \frac{2}{\eta k_5^2} = \frac{32\pi^6 c(T, \mu_e)}{9\zeta(3)^2 e^4 g_b^2 \eta} \left(\frac{\delta\rho}{\rho} \frac{\Gamma_w}{\Gamma_f} T^3 \right)^{-2}. \quad (3.1)$$

We first analyze the case for which the density fluctuations are close to the average density $\delta\rho \sim \rho$ and then consider that $\delta\rho$ is lower than ρ by one order of magnitude. After the initial 10 seconds of its life, the neutron star becomes transparent to neutrinos and the magnetic field amplification can be estimated by putting $\delta\rho/\rho = 1$.

In fig. 2 the evolution of the chiral magnetic instability with a vanishing initial value for the chiral chemical potential is shown and table 1 contains the respective $|\mu_{5,b}|$, Γ_w^{-1} , Γ_f^{-1} , t_{damp} and k_5^{-1} values taking $\delta\rho/\rho = 1$.

From (2.41), the maximum field strength that can be reached by the instability is independent of the initial magnetic seed field. Its strong temperature dependence reflects the fact

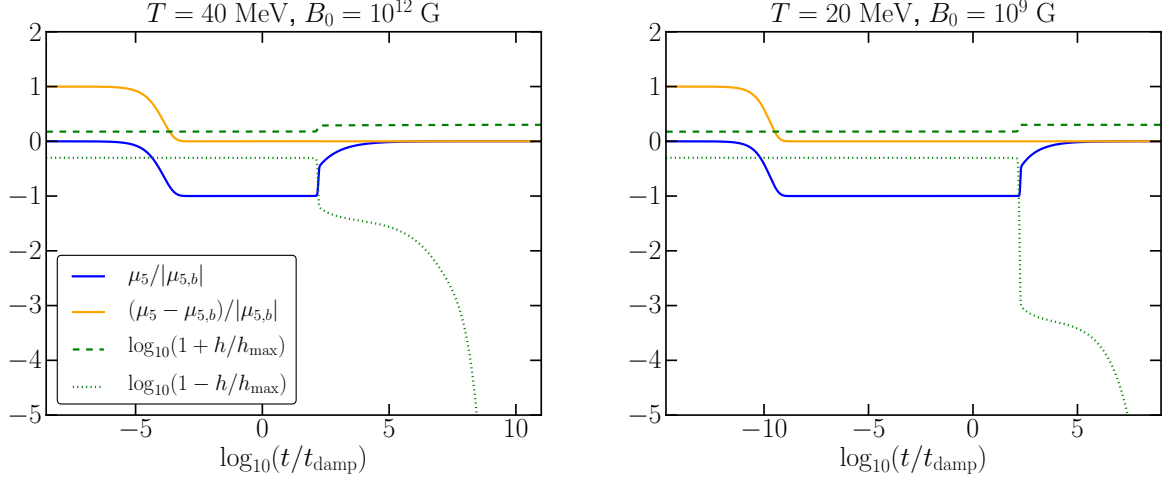


Figure 2. Time evolution of the chiral chemical potential normalized to the equilibrium value, $\mu_5/|\mu_{5,b}|$, relative difference of the chiral chemical potential to the equilibrium value, $(\mu_5 - \mu_{5,b})/|\mu_{5,b}|$ and, in logarithmic units, relative deviation of the helicity density from its maximal and minimal value, $1 \pm h/h_{\max}$. The left panel is for a temperature of $T = 40$ MeV and seed field $B_0 = 10^{12}$ G, and the right panel is for $T = 20$ MeV and a seed field of $B_0 = 10^9$ G.

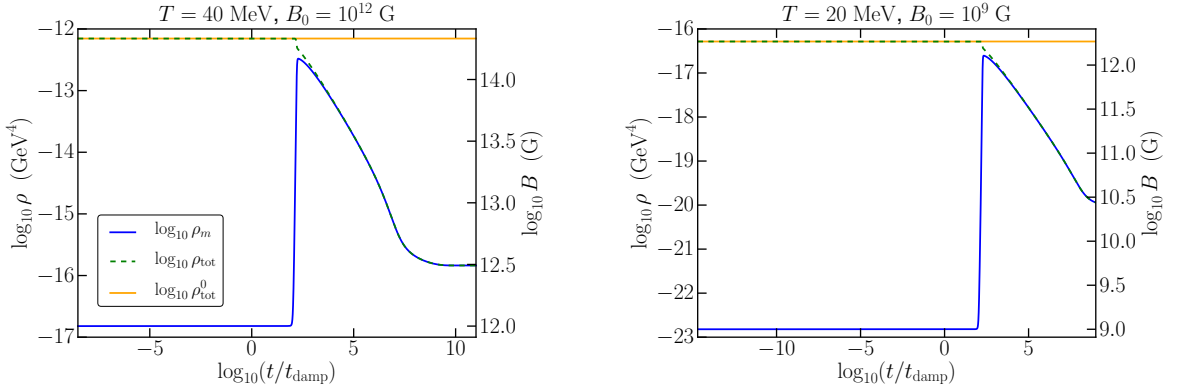


Figure 3. Time evolution of the magnetic energy density ρ_m and total energy density ρ_{tot} . Also shown is the initial total energy density which limits the maximal magnetic energy density that can be reached by the instability. In the left panel $T = 40$ MeV and in the right panel $T = 20$ MeV.

T (MeV)	$ \mu_{5,b} $ (MeV)	Γ_w^{-1} (s)	Γ_f^{-1} (s)	t_{damp} (s)	k_5^{-1} (cm)	B_{max} (G)
40	2×10^{-3}	1×10^{-9}	3×10^{-12}	6×10^{-8}	3×10^{-6}	8×10^{14}
20	4×10^{-6}	9×10^{-8}	3×10^{-12}	0.04	1×10^{-3}	1×10^{13}

Table 1. Equilibrium chiral asymmetry (2.40), chiral asymmetry creation and depletion rates (2.2) and (2.5), respectively, damping time (3.1) and characteristic scale (2.40) values for $\delta\rho/\rho = 1$. Maximal magnetic field amplification computed using (2.41).

that Γ_w has a stronger dependence on temperature than Γ_f , which means that the higher the temperature, the higher the magnitude of μ_5 and the sooner the chiral magnetic instability develops and subsequently damps. The values predicted for the maximal field strength

(2.41) are listed in the last column of table 1. For the examples we chose magnetic seed fields $B_0 = 10^{12}$ G for $T = 40$ MeV and $B_0 = 10^9$ G for $T = 20$ MeV to illustrate how the magnetic field amplification is limited by energy conservation when the magnetic energy gets close to the maximum allowed value. In fig. 3, for $T = 40$ MeV the magnetic energy density grows steeply up to close to the total energy of the system, corresponding to $B_{\max} \simeq 1 \times 10^{14}$ G, within a few μs and subsequently the magnetic field decreases by a factor of more than 10 within a few seconds. For $T = 20$ MeV, the magnetic field grows within about 4 seconds up to $B_{\max} \simeq 1 \times 10^{12}$ G.

The total energy density

$$\rho_{\text{tot}} \simeq \frac{T^2}{6} \left(\mu_5^2 + 2 \frac{\Gamma_f}{\Gamma_w} \mu_{5,b}^2 \right) + \rho_m, \quad (3.2)$$

includes the energy density ρ_5 from (2.29), the energy corresponding to the background particles coupling to the chiral electrons from (2.35) which ensures that the total energy due to the scattering terms is conserved, and the magnetic energy density ρ_m . The initial total value is not exceeded and, as predicted, ρ_{tot} decreases only due to resistive damping following the dissipation of ρ_m . The number of wavenumber modes considered is sufficiently large for the decay of the magnetic energy to correspond to a smooth curve. The decay changes ρ_m roughly linearly with time, as expected from the discussion in Sect. 2.3.

The chiral asymmetry is built up through the capture of left-handed electrons until an equilibrium with the spin-flip processes is reached at $\mu_5 = \mu_{5,b}$. When the magnetic field starts to be amplified, the term in (2.19) proportional to the magnetic helicity will eventually dominate. At this point the asymmetry μ_5 will start to decrease as chiral energy is transferred into magnetic energy.

The curve $(\mu_5 - \mu_{5,b})/|\mu_{5,b}|$ in fig. 2 is very close to zero after the equilibrium value is reached, which implies that when the magnetic field terms begin to dominate the evolution of μ_5 and $\mu_{5,b}$ occurs in lockstep. The chiral chemical potential grows and reaches equilibrium at a value close to $\mu_{5,b}$ until the magnetic field term starts to dominate and depletes the chiral asymmetry. The scattering of electrons, covered by the term proportional to $\mu_{5,b}$ does not allow for μ_5 to be replenished.

The magnetic helicity density, normalized to the maximal value $h_{\max}(k) = (8\pi/V)(M_k/k)$, depends on the mode considered and maintains its initial value, here simply chosen as $h^0 = h_{\max}/2$, until the amplification of the magnetic field makes it either grow to its maximum or decay, if the sign between helicity and μ_5 is the opposite or equal, respectively. Thus, fields amplified by the chiral instability turn into maximally helical fields. Furthermore, once magnetic field growth sets in the evolution is essentially independent of the initial helicity.

It is also interesting to compute how the magnetic field power spectrum evolves with time. Fig. 4 shows the time evolution of the magnetic field power spectrum for a flat and a Kolmogorov initial spectrum. As expected, the final magnetic field power spectrum is not very sensitive to the initial magnetic field power spectrum. The magnetic field power spectrum peaks at wavenumbers close to $k_5/2$, while it decays with time due to resistive damping for $k > k_5$. Since k_5 is proportional to the evolving chiral chemical potential μ_5 , see (2.24), which decreases for $\log_{10}(t/t_{\text{damp}}) > 2$, first steeply and then smoothly, see fig. 2, with growing time the peak in the magnetic power spectrum moves to smaller k . This is reflected in fig. 4 which also shows that the total magnetic energy grows exponentially for times $\simeq 10^2 t_{\text{damp}} \lesssim t \lesssim 10^3 t_{\text{damp}}$, then saturates and gets damped for subsequent times.

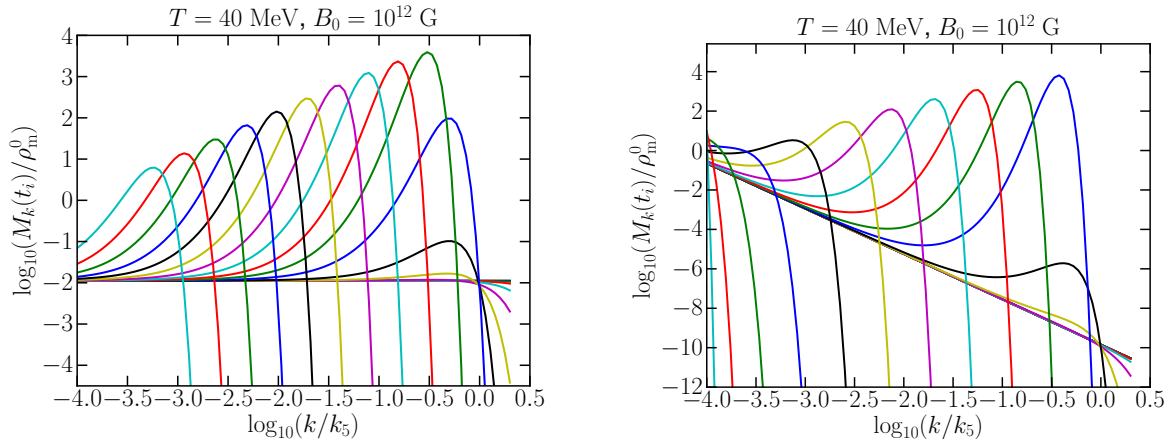


Figure 4. Time evolution of the magnetic field power spectrum normalized to the initial magnetic energy density, M_k/ρ_m^0 , as a function of wavenumber k normalized to k_5 . The power spectra are shown for equally spaced intervals in the logarithm of time between $t = t_{\text{damp}}$ and $t = 10^8 t_{\text{damp}}$, for $T = 40$ MeV. Left panel: Initially flat power spectrum. Right panel: Initial power spectrum has a Kolmogorov distribution.

In the simulations of the magnetic field power spectra we considered the most relevant modes k for magnetic amplification: The peak of the magnetic field power spectrum yields a maximal growth for $k_5/2$ and taking into account much smaller wavenumber modes up to the size of the neutron star radius, $k \sim 1/(10 \text{ km})$, does not significantly change our results.

We can also estimate the time dependence of k_5 in the damping regime: Eq. (2.15) shows that amplification stops and resistive damping sets in when $2\eta k_5^2 t \sim 1$. Therefore, we expect the scaling

$$k_5 \sim k_5^0 \left(\frac{t_0}{t} \right)^{1/2}, \quad \mu_5 \sim \mu_5^0 \left(\frac{t_0}{t} \right)^{1/2}, \quad (3.3)$$

where k_5^0 and μ_5^0 are the values of k_5 and μ_5 , respectively, at $t \simeq t_{\text{damp}}$. Fig. 4 allows us to estimate the length scale at which the power spectrum peaks after the magnetic field growth ends. For $T = 40$ MeV we obtain $k^{-1} \simeq 0.1 \text{ mm}$ while for $T = 20$ MeV we find $k^{-1} \simeq 3 \text{ cm}$. This is significantly smaller than the neutrino mean free path discussed in Sect. 2.5. Therefore, in the presence of significant density fluctuations on these length scales we expect that magnetic field growth due to the chiral magnetic instability is possible.

Let us finally turn our attention to the case involving density fluctuations $\delta\rho/\rho = 0.1$ in the core of the neutron star, as illustrated in fig. 5 for seed magnetic fields of 10^9 G . For $T = 40$ MeV one obtains a field amplification of now only $\simeq 1 \times 10^{13} \text{ G}$, whereas for 20 MeV it yields $\simeq 2 \times 10^{11} \text{ G}$.

3.1 Neutrino sphere and cold neutron star

If we consider the typical radius of a neutron star to be 10 km, the density at the neutrino sphere is $\sim 10^{11} \text{ g cm}^{-3}$. The lepton fraction can be roughly taken as $Y_L \sim 0.1$ [26] and the average neutrino energy is at most 16 MeV [27], which translates to a temperature of $T \sim E_\nu/3 \sim 5 \text{ MeV}$. At this and lower temperatures, an additional particle is required for electron capture to occur, similarly to the modified URCA process $N + p + e_L \rightarrow N + n + \nu_{eL}$,

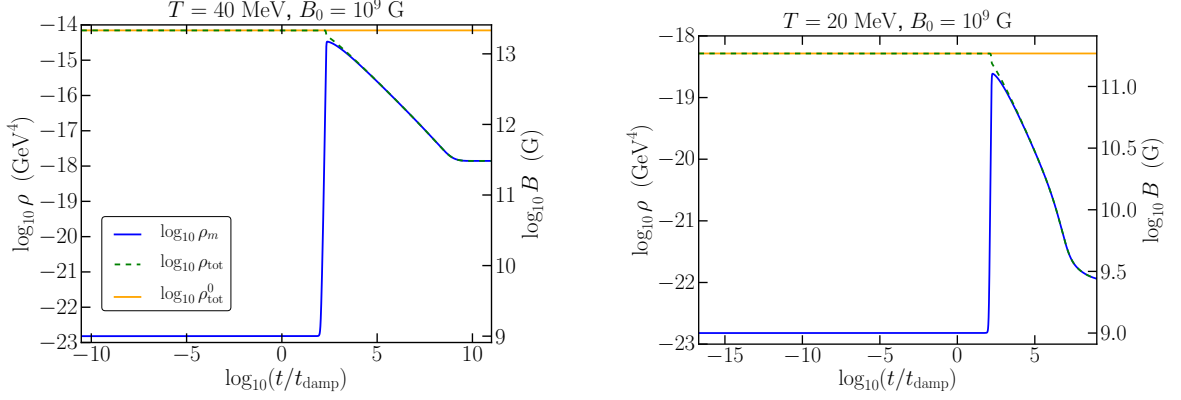


Figure 5. Energy densities obtained when the factor $\delta\rho/\rho = 0.1$ is included, accounting for the density fluctuations in the neutron star core.

where N can be either a neutron or a proton. The estimate (2.22) gives a chiral asymmetry of $|\mu_{5,b}| \sim 10^{-12}$ MeV which in turn through (2.41) gives negligible maximal magnetic fields.

Let us now briefly concentrate on mature neutron stars of about 10^5 years old, where the core temperature drops to typically 2×10^8 K and the main cooling mechanism is surface photon emission [25]. The URCA rate yields an also very small instability equilibrium value $|\mu_{5,b}| \sim 10^{-32}$ MeV, which in turn corresponds to a field growth only around extremely small k and in extremely large time scales, indicating that the chiral asymmetry is also not effective in generating magnetic fields for this regime. We, therefore, obtain significant magnetic field amplification only during the hot initial phase of the neutron star. This is in contrast to [15, 16] which included the difference in the forward scattering amplitudes for left and right chiral electrons which gives rise to a constant potential term V_5 . These authors effectively introduced the rescaling $\mu_5 \rightarrow \mu_5 + V_5$ in the terms involving the magnetic field but not in the terms for the chiral asymmetry evolution due to interactions with the background, yielding an artificial steady source of magnetic energy. However, in our opinion this rescaling should be performed in all terms so that it only introduces a constant shift of μ_5 which can be eliminated by redefining μ_5 . In other words, the thermodynamic equilibrium abundances can only depend on the total chiral energy difference $\mu_5 + V_5$, and not only on μ_5 . As a result, V_5 should affect neither the scale nor magnitude of the magnetic field amplification. In contrast, if only the kinetic part of μ_5 would be given by (2.22), substituting $\mu_{5,bi} \rightarrow \mu_{5,bi} + V_5$ in (2.36) and using $\mu_{5,bi} \simeq \mu_{5,b}$ with (2.22) would yield

$$\rho_m \lesssim c(T, \mu_e) \frac{\Gamma_f}{\Gamma_w} \left(0.09 \frac{\Gamma_w}{\Gamma_f} \frac{T^3}{c(T, \mu_e)} + V_5 \right)^2. \quad (3.4)$$

But since $\Gamma_w \propto G_F^2$ and $V_5 \propto G_F$ this would not vanish in the limit of $G_F \rightarrow 0$, as is expected since if parity is conserved and there is no chiral asymmetry, the energy associated with the chiral asymmetry should vanish. This indicates that the evolution of the system should not depend on V_5 . The consideration of a term of this kind has been also discussed and discarded in [14, 29] under similar reasoning. In Ref. [28] the authors claim that the maximal magnetic field energy density $B_{eq}^2/(8\pi)$ is given by the thermal energy of the nucleons and electrons but no derivation is given and it is unclear how this is related to V_5 . Furthermore, saturation of magnetic field growth is introduced ad hoc by substituting $\mu_5 + V_5 \rightarrow (\mu_5 + V_5)/(1 + B^2/B_{eq}^2)$ without derivation.

4 Summary and conclusions

In a supernova core collapse electron capture creates an imbalance between left- and right-handed electrons $\mu_5 \sim \text{eV} - \text{keV}$. It has been suggested that the chiral anomaly can transform the energy associated with this chiral imbalance into the growth of helical magnetic fields, possibly up to the high values that have been observationally inferred for neutron stars and magnetars. In the present work we investigated this possibility within a semi-analytical approach with specific emphasis on the evolution of the total energy which can only decrease or stay constant and thus limits the maximally possible magnetic field strength. While neutrinos are trapped in the core, density fluctuations allow for local thermodynamic disequilibrium between URCA and inverse URCA rates due to neutrino free-streaming on sufficiently small length scales $\ell_\nu \sim \text{cm}$, which prevents this imbalance to be washed out by the inverse reactions. For length scales $10^{-6} \text{ cm} \lesssim \pi/(2e^2|\mu_5|) \lesssim \ell_\nu \lesssim 15 \text{ cm}$ the chiral magnetic effect can then create magnetic fields of roughly maximal helicity on time scales short compared to the evolution of the neutron star before they saturate due to the limited energy associated with the chiral lepton asymmetry.

For a core temperature of 40 MeV, we obtain maximal magnetic field strengths $B_{\text{max}} \sim 10^{14} \text{ G}$ on tens of nanometer length scales reached within microseconds. For lower temperatures, such as 20 MeV, the magnetic fields are smaller and concentrated on larger length scales, and the growth rates are lower. This suggests that the range of field strengths and power spectra due to the chiral magnetic instability depend on the initial temperature of the protoneutron star. The generated fields are not strong enough to account for typical magnetar field strengths and tend to be produced on submillimeter length scales rather than dipolar fields on the linear scale of the star. We also find that outside the neutrino sphere, as well as in a cold neutron star at temperatures below $\simeq 10 \text{ MeV}$, the chiral instability can not lead to significant field amplification, due to the fact that lower temperatures imply smaller asymmetry values μ_5 .

We briefly summarize the differences between our study and other recent work on the chiral magnetic instability in neutron stars. Maximum surface fields of 10^{18} G were estimated in Ref. [5] by considering a very high and constant $\mu_5 = 200 \text{ MeV}$. The procedure in Ref. [14] yields a chiral asymmetry $\sim 10^{-12} \text{ MeV}$ (for $T = 30 \text{ MeV}$), several orders of magnitude lower than our result motivated by the electroweak electron capture rate. The responsible mechanism for the magnetic field growth in Ref. [15, 16, 28] is stated as being due to a potential term V_5 that accounts for the parity asymmetric forward scattering of chiral electrons and nucleons and which acts on a much longer time scale, being relevant for cold neutron stars. In our treatment any chiral asymmetry in the forward scattering of electrons on background species does not separately contribute to the enhancement of the magnetic field because only the total asymmetry energy $\mu_5 + V_5$ should enter the evolution equations, as also concluded in Ref. [14, 29]. We rather believe that the magnetic field evolution only depends on the asymmetry between left- and right-handed electron abundances which in turn is a function of the ratio of electroweak URCA and spin flip rates.

One important approximation taken throughout this work was neglecting the role that turbulence may play in suppressing the chiral instability by setting $\mathbf{v} = 0$ in the MHD equation. This should be a good approximation as long as the velocity field is sufficiently smooth on the instability length scales or the power index sufficiently large, as shown in A, which allows to transform into an inertial frame moving along with the plasma. We also consider the temperature and the resistivity of a protoneutron star to be constant over

the first initial stage of evolution after the supernova collapse. The later should be a good approximation since for $T \gtrsim 20$ MeV all relevant time scales, including the instability growth scale, are short compared to the scale on which the temperature changes, which is a few seconds [17]. Lower temperatures imply instability time scales longer than a few seconds on which the cooling of the protoneutron star should be taken into account. The resistivity that we employed in this work assumes that particles in the protoneutron star core are degenerate whereas a semi-degenerate regime is more realistic. This affects the resistive damping rate and thus the damping time and the timescale in which the instability grows. Additionally, since the instability timescale is in any case small compared to the dynamical timescale, the final state, in particular the finite magnetic field strength, is not influenced by this uncertainty because it is determined by saturation of the magnetic field energy at a value comparable to the energy in the chiral asymmetry and given by eq. (2.37).

Acknowledgments

We thank V. Semikoz for useful discussions. This work was supported by the "Helmholtz Alliance for Astroparticle Physics (HAP)" funded by the Initiative and Networking Fund of the Helmholtz Association and by the Deutsche Forschungsgemeinschaft (DFG) through the Collaborative Research Centre SFB 676 "Particles, Strings and the Early Universe".

A The role of turbulence

In this section we show under which conditions the assumption that the fluid turbulence can be neglected is a good approximation. Comparing the first and third terms of (2.11) provides us with an estimate of how large the velocity in the core of a protoneutron star has to be to dominate over the chiral term in the MHD equation studied in the present work. Let us assume a fluid velocity spectrum of the form

$$\langle \mathbf{v}^2(T, k) \rangle = \mathbf{v}_i^2(T) \left[\frac{k}{k_i(T)} \right]^n, \quad (\text{A.1})$$

with k_i being the inertial wavenumber. In terms of the length scale $\ell = 2\pi/k$ and of the root-mean-square velocity $\mathbf{v}_{\text{rms}} = \sqrt{\langle \mathbf{v}^2(T, k) \rangle}$, this gives us for the velocity flow

$$\mathbf{v}_\ell = \mathbf{v}_{\text{rms}} \left(\frac{\ell}{L} \right)^{n/2}, \quad (\text{A.2})$$

with L the integral length scale and n the power index. From the MHD equation with the chiral anomaly (2.11), the velocity and anomalous term can be estimated as

$$\begin{aligned} \nabla \times (\mathbf{v} \times \mathbf{B}) &\sim \frac{vB}{\ell}, \\ \frac{e^2}{2\pi^2\sigma} \mu_5 \nabla \times \mathbf{B} &\sim \frac{e^2 \mu_5 B}{2\pi^2 \sigma \ell}, \end{aligned} \quad (\text{A.3})$$

such that the relative importance of the first is roughly dictated by

$$\frac{\nabla \times (\mathbf{v} \times \mathbf{B})}{e^2/(2\pi^2\sigma) \mu_5 \nabla \times \mathbf{B}} \sim 2\sigma L v_{\text{rms}} \left[\left(\frac{e}{\pi} \right)^2 L \mu_5 \right]^{-(n/2+1)}, \quad (\text{A.4})$$

by considering that the relevant scale for the instability is $\ell = 2\pi/k_5 = (\pi/e)^2|\mu_5|^{-1}$.

We take the example of a protoneutron star with $T = 40$ MeV, with a corresponding conductivity of $\sigma \simeq 0.21$ GeV computed from (2.4), that according to table 1 has an electron chiral chemical potential of 2×10^{-3} MeV. Considering the scale at which most energy will be concentrated after the hot cooling phase being $L \sim \text{km}$, for a Kolmogorov velocity spectrum ($n = 2/3$), we obtain

$$\frac{\nabla \times (\mathbf{v} \times \mathbf{B})}{e^2/(2\pi^2\sigma)\mu_5 \nabla \times \mathbf{B}} \simeq 5 \times 10^3 v_{\text{rms}}. \quad (\text{A.5})$$

This implies that for $n = 2/3$, the effect of the chiral instability dominates unless the fluid velocity of the protoneutron star core is $v_{\text{rms}} \gtrsim 10^{-4}$. As an upper limit to the typical velocities implied we consider the example of 4×10^8 cm/s [24], rendering $v_{\text{rms}} \simeq 10^{-2}$, which indicates that in this regime our results do not apply for Kolmogorov turbulence, but only for larger power indices, such as $n = 4/3$ in this case. For a lower limit on the fluid velocity we take the example of 10^5 cm/s [30], giving $v_{\text{rms}} \simeq 3 \times 10^{-6}$, which according to (A.5) shows that the MHD equation will be dominated by the chiral anomaly for a Kolmogorov type spectrum in this case.

The velocity term in the MHD equation becomes less important as n increases: for a Kraichnan type spectrum ($n = 1$), (A.4) is of the order unity and smaller for $v_{\text{rms}} \lesssim 10^{-3}$. The previous estimates make clear that turbulence can be neglected for relatively small fluid velocities or large power indices, but that depends on the details of the velocity spectrum at play in the core of the protoneutron star.

References

- [1] R. C. Duncan and C. Thompson, *Astrophys. J.* **392**, L9 (1992).
- [2] C. Kouveliotou *et al.*, *Nature* **393**, 235 (1998).
- [3] S. A. Olausen and V. M. Kaspi, *Astrophys. J. Suppl.* **212**, 6 (2014) [arXiv:1309.4167 [astro-ph.HE]].
- [4] L. Ferrario, A. Melatos and J. Zrake, arXiv:1504.08074 [astro-ph.SR].
- [5] A. Ohnishi and N. Yamamoto, arXiv:1402.4760 [astro-ph.HE].
- [6] K. Fukushima, D. E. Kharzeev and H. J. Warringa, *Phys. Rev. D* **78**, 074033 (2008) [arXiv:0808.3382 [hep-ph]].
- [7] Y. Akamatsu and N. Yamamoto, *Phys. Rev. D* **90**, no. 12, 125031 (2014) [arXiv:1402.4174 [hep-th]].
- [8] A. Boyarsky, J. Frohlich and O. Ruchayskiy, *Phys. Rev. Lett.* **108**, 031301 (2012) [arXiv:1109.3350 [astro-ph.CO]].
- [9] H. Tashiro, T. Vachaspati and A. Vilenkin, *Phys. Rev. D* **86**, 105033 (2012) [arXiv:1206.5549 [astro-ph.CO]].
- [10] M. Kaminski, C. F. Uhlemann, M. Bleicher and J. Schaffner-Bielich, arXiv:1410.3833 [nucl-th].
- [11] M. Dvornikov, *Phys. Rev. D* **90**, no. 4, 041702 (2014) [arXiv:1405.3059 [hep-ph]].
- [12] M. Dvornikov and V. B. Semikoz, *JCAP* **1405**, 002 (2014) [arXiv:1311.5267 [hep-ph]].
- [13] M. Dvornikov, arXiv:1409.1463 [hep-ph].
- [14] D. Grabowska, D. B. Kaplan and S. Reddy, *Phys. Rev. D* **91**, no. 8, 085035 (2015) [arXiv:1409.1463 [hep-ph]].

- [15] M. Dvornikov and V. B. Semikoz, Phys. Rev. D **91**, no. 6, 061301 (2015) [arXiv:1410.6676 [astro-ph.HE]].
- [16] M. Dvornikov and V. Semikoz, JCAP **1505**, 32 (2015) [arXiv:1503.04162 [astro-ph.HE]].
- [17] A. Burrows and J. M. Lattimer, Astrophys. J. **307**, 178 (1986).
- [18] J. M. Lattimer, M. Prakash, C. J. Pethick and P. Haensel, Phys. Rev. Lett. **66**, 2701 (1991).
- [19] B. Friman and O. Maxwell, Astrophys. J. **232**, 541 (1979).
- [20] G. Baym, C. J. Pethick and D. Pikes Nature **224**, 674 (1969).
- [21] J. Ahonen and K. Enqvist, Phys. Lett. B **382**, 40 (1996) [hep-ph/9602357].
- [22] A. Boyarsky, J. Frohlich and O. Ruchayskiy, Phys. Rev. D **92**, no. 4, 043004 (2015) [arXiv:1504.04854 [hep-ph]].
- [23] N. Iwamoto, Annals Phys. **141**, 1 (1982).
- [24] J. Mao, M. Ono, S. Nagataki, M. Hashimoto, H. Ito, J. Matsumoto, M. G. Dainotti and S.-H. Lee, Astrophys. J. **808**, no. 2, 164 (2015) [arXiv:1507.07061 [astro-ph.HE]].
- [25] G. G. Raffelt, Chicago, USA: Univ. Pr. (1996) 664 p.
- [26] A. Sulaksono and L. Satiawati, Phys. Rev. C **87**, no. 6, 065802 (2013).
- [27] H.-T. Janka and W. Hillebrandt, Astrophys. J. **78**, 375 (1989).
- [28] M. Dvornikov and V. B. Semikoz, arXiv:1507.03948 [astro-ph.HE].
- [29] A. Vilenkin Phys. Rev. D **22**, 3067 (1980)
- [30] B. Link, Mon. Not. Roy. Astron. Soc. **422**, 1640 (2012) [arXiv:1105.4654 [astro-ph.SR]].